Identification of Nonlinear Excitation Force Kernels Using Numerical Wave Tank Experiments

Simone Giorgi, Josh Davidson and John V. Ringwood
Centre for Ocean Energy Research
Maynooth University, Co.Kildare, Ireland
simone.giorgi@eeng.nuim.ie
josh.davidson@eeng.nuim.ie
john.ringwood@eeng.nuim.ie

Abstract—This paper addresses the mathematical modelling of the relationship between the free surface elevation (FSE) and the excitation force for wave energy devices (excitation force model). While most studies focus on the model relating the FSE to the device motion, the excitation force model is required to complete the mathematical wave energy system description and also plays an important role in excitation force observer design. In the paper, a range of linear and nonlinear modelling methodologies, based on system identification from numerical wave tank tests, are developed for a range of device geometries. The results demonstrate a significant benefit in adopting a nonlinear parameterisation and show that models are heavily dependent on incident wave amplitude.

Index Terms—Excitation force, System identification, Numerical wave tank, Wave energy, Discrete-time modelling, ARX model, Hammerstein model, Kolmogorov-Gabor Polynomial Model

I. INTRODUCTION

Mathematical modelling of wave energy converters (WECs) has many uses, including simulation of device motion, power production assessment and as a basis for model based control design. A large number of models employed in the simulation and analysis of WECs are based on the Cummins equation [1]. Cummins' equation is based on Newton's second law describing the motion of the device floating in water subjected to the fluid, gravity and other external forces (like the mooring force, f_M, and the PTO force, f_{PTO}). The fluid force is derived under the simplifying hypothesis of linear potential theory, that allows the total fluid force (applied from the fluid to the floating body) to be written as the summation of the excitation force, f_E, the radiation force, f_{RAD}, and the buoyancy force, f_{BU}, and to express the radiation force as a convolution integral. Therefore, the structure of the model can be graphically represented using the block diagram of Fig. 1, where $f_{IN} = f_M + f_E + f_{PTO}$ represents the right hand side of the Cummins equation [2].

When the body is in motion, the excitation force is not directly measurable; however, the excitation force is a vital variable required by energy maximising control systems [3] and, in the absence of a direct measurement, a suitable estimate is required, which can be provided by an observer [4]. In a typical observer configuration, [5], a model linking the input with the variable to be estimated (documented in this paper),
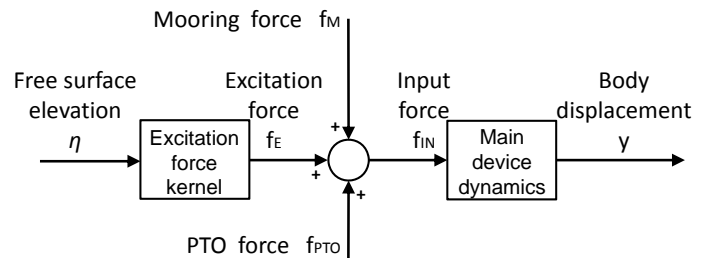

Fig. 1. General block diagram of the wave energy device model.

along with the model linking the variable to be estimated with the system output (see, for example [6]) needs to be provided. In this paper, the attention is focused on the modelling of the relationship between the undisturbed free surface elevation (FSE), η, measured in a position that corresponds to the centre of mass of the body, and the excitation force, that is the force experienced by the body when it is held fixed in the presence of waves [7]. This relationship is represented by the "Excitation force kernel" block in Fig. 1.

In the context of linear models, the relationship between η and f_E can be described in the time domain via a convolution integral or, in frequency domain, with a transfer function [8]. Linear models have very desirable properties, like superposition or a frequency domain description, but they are based on the hypothesis of small waves, ideal fluid (inviscid and incompressible) and small body displacement, that are not satisfied in reality for the wave energy context. Consequently, when the wave amplitude increases, becoming of the same order of magnitude of the dimensions of the body, some nonlinear effect may appear. As an example, Fig. 2 shows the excitation force experienced from a fixed body subjected to monochromatic waves; it is shown that, despite the fact that the sinusoidal input is symmetrical with respect to the mean free surface elevation (MFSE), the excitation force is asymmetric. Furthermore, Fig. 3 shows that there is a nonlinear relationship between the incident wave and excitation force amplitudes. Such typical nonlinear effects are an indication that it is necessary to introduce nonlinearities into the models utilised to describe the interaction between the body and the fluid.
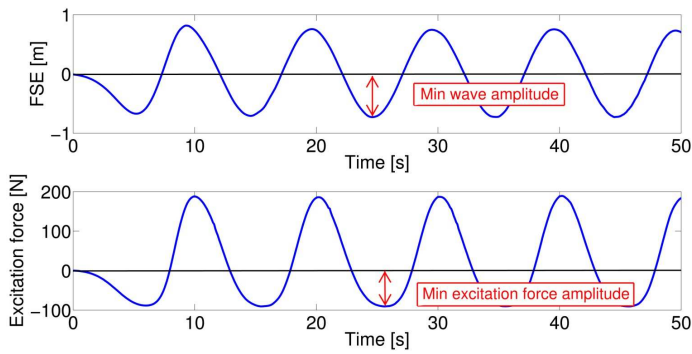
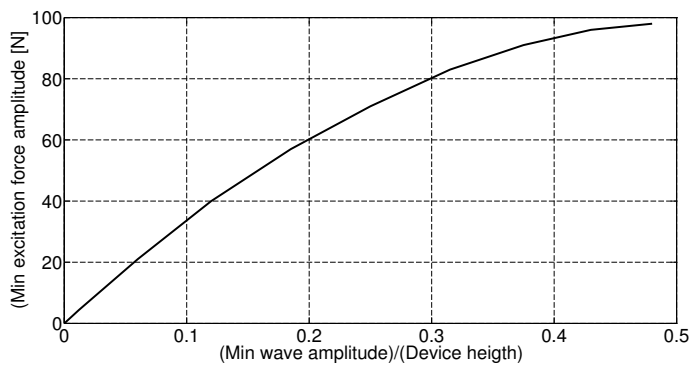Fig. 2. Regular FSE and excitation force time series.

Fig. 3. Max excitation force amplitude vs (max wave amplitude)/(Device heigth).

Different studies have already been conducted to introduce nonlinear effects into the calculation of the excitation force, taking into consideration the fact that the wetted surface of the body is not constant in time, as assumed by linear potential theory, but changes depending on the FSE and the position of the body. Therefore, the excitation force has been calculated by integrating the pressure on the instantaneous wetted surface of the body [9]–[12].

An alternative modelling approach, utilised in this paper, is that of system identification, where models are determined from input/output data measured from the system under study [13]. Such methods are particularly useful where the system to be modelled is very complex and/or does not easily lend itself to first principles modelling. However, one major difficulty in system identification is ensuring that the input/output data used to determine the model is sufficiently representative of the system dynamics and, in particular, must cover the range of frequencies and amplitudes likely to be encountered during system operation. In the WEC case, such a range of excitation signals are not likely to be available in the open ocean (at least not in a reasonably short time frame) and there are difficulties in exactly enumerating the excitation experienced by the device, particularly for a directional device. In short, in the open ocean, there is no external control of the excitation. One other possibility is to employ tank tests. However, in addition to the significant cost and the need for a physical

prototype, there may be limitations on the range of excitation signals available and tank wall reflections may further limit the range and duration of viable tests.

A different option for generating suitable input/output data is to use a numerical wave tank (NWT), implemented in CFD [6], which has the following advantages :
- Reflections from tank walls can be effectively controlled,
- The device can be tested at full scale, eliminating scaling effects,
- A wide variety of excitation signals, including incident waves and forces directly applied to the device, as well as free response tests, can be implemented,
- The device can be constrained to different modes of motion without requiring mechanical restraints, which can add friction and alter the device dynamics,
- Signals can be passively measured without requiring physical sensor devices which can alter the device or fluid dynamics and are subject to measurement error and, most importantly,
- Specialist equipment, including a prototype WEC device, is not required.

In this paper, for simplicity, the general six degree of freedom (DOF) problem has been reduced to a heave single DOF. However, the illustrated methods and procedures can be extended to the full six DOF.

The paper is laid out as follows; in Section II, the structure of the proposed linear and nonlinear models are outlined. Section III then explains the NWT experiments used to produce the system identification data. Section IV describes the process of identifying the model parameters from the NWT generated data. Some illustrative examples demonstrating these methods are then given in Section V, and the results of the different models compared.

II. MODEL STRUCTURES

A. General Dynamic Model Structure

Choice of the parametric structure of the model is very important, if a representative model is to be identified. The model structure may be inspired from physical system knowledge and considerations (white-box modelling) or completely based on the recorded data itself (black-box modelling). There are also many possibilities within these two extremes which are denoted by shades of grey e.g. off white, slate grey, smoke grey, etc [14]. In general, whether the model structure is inspired by physical phenomena or purely derived from the data, it is necessary to determine a *parsimonious* structure for the model which will work well with the identification data, but also generalise well to other data. A compatible requirement is that it is not desirable to add complexity to the model for little gain. The identified parametric model should be able to capture the essential nonlinearities, but remain, simultaneously, with a sufficient simplicity that allows the model to be run in real time.

Considering the discrete time nature of sampled data from experiments, the majority of system identification techniques are based on discrete time models [13]. For this reason, discrete time models are utilised in this paper. However,
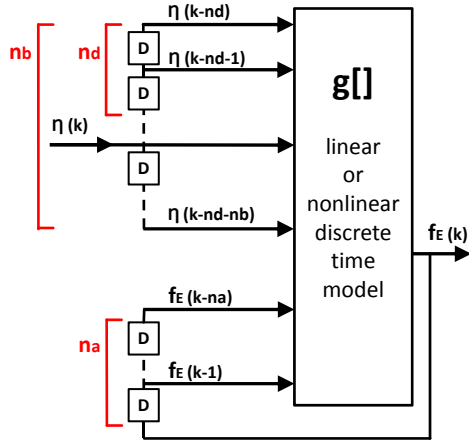
Fig. 4. Block diagram for a general NARX discete-time model. Each D-block denotes a single delay element. n_a, n_b and n_d indicate the number of D-blocks.

identification of continuous time models can also be performed [15] [16]. Discrete-time modelling implies using signals only at the discrete time instants $t = kT_s$, where T_s is the sampling period and k is an integer. The values of the η and f_E at the time instant kT_s are represented with the symbols $\eta(k)$ and $f_E(k)$ respectively.

The relationship between η and f_E is non causal [8], therefore, noncausality has to be introduced into the structure of the identified model. In this paper, models with external dynamics, called nonlinear autoregressive with exogenous input (NARX) models [17], are utilized. In NARX models, the present value of the output $f_E(k)$ depends on the past values of the output $f_E(k-1), ..., f_E(k-n_a)$ and the input values $\eta(k-n_d), \eta(k-n_d-1), ..., \eta(k-n_d-n_b)$. If the system is causal, the output does not depend on future values of the input and $n_d \geq 0$, otherwise, if the system is noncausal, $n_d < 0$ and the present value of the output is influenced by future input values. The NARX model is summarized with the following equation:

$$y(k) = g\Big[f_E(k-1), ..., f_E(k-n_a),$$
$$\eta(k-n_d), \eta(k-n_d-1), ..., \eta(k-n_d-n_b)\Big] \quad (1)$$

which can be represented with the block diagram of Fig. 4. n_a and n_b represent the dynamical order of the model, and increasing them, the model becomes more flexible and able to show more complex behaviour, but, at the same time, unnecessarily high orders can make the model less able to generalise on new data (overfitting). n_d is the input delay time and it represents the number of samples before the output reacts to the input (for $n_d \geq 0$) or the number of future input steps that influence the present value of the output (for $n_d < 0$).

B. ARX Model (Linear)

The first parametric model utilised in this paper is the autoregressive with exogenous (ARX) model. It is a well
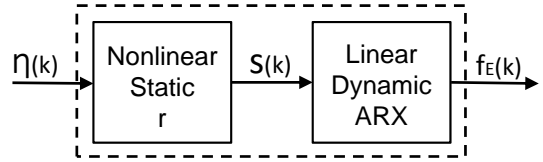

Fig. 5. Block diagram of the Hammerstein model.

known black box model with a linear input-output relationship and is linear in the parameters a_i and b_i. For the ARX model, Equation (1) becomes:

$$f_E(k) = \sum_{i=1}^{n_a} a_i f_E(k-i) + \sum_{i=0}^{n_b} b_i \eta(k-n_d-i) \quad (2)$$

C. Hammerstein Model (Nonlinear)

A way to introduce a nonlinearity into the relationship between the input $\eta(k)$ and the output $f_E(k)$ of the model is to utilise a nonlinear static block. The Hammerstein model consists of a cascade connection of a nonlinear static block followed by a linear dynamic block (see Figure 5). In the Hammerstein case, Equation (1) becomes [18]:

$$f_E(k) = \sum_{i=1}^{n_a} a_i f_E(k-i) + \sum_{i=0}^{n_b} b_i r[\eta(k-n_d-i)] \quad (3)$$

where $r[.]$ is a nonlinear static function. The Hammerstein model is characterized by a nonlinear input-output relationship, but is linear in the parameters a_i and b_i. In the Hammerstein model, the static relationship between input and output is given by the product of the static function, $r[.]$, and the steady-state gain of the ARX model, DC_{gain}. Therefore, the characterization of the two blocks is not unique, any pair $(DC_{gain}/\alpha , \alpha r)$ will produce the same input and output [19]. To remove this ambiguity, the DC_{gain} of the ARX block is set to unity, which allows the steady-state gain for the entire Hammerstein model to be solely represented by the nonlinear static function. In this case, $r[\eta(k)]$ will represent the static relationship between the constant input free surface elevation and the constant output excitation force, which is just the buoyancy force. Therefore, once the buoyancy force versus constant wave elevation relationship is available, the nonlinear static function, $r[.]$, can be identified separately from the linear dynamic block. In this way, the Hammerstein model black-box structure is given a shade of 'grey' by considering the physical meaning of the nonlinear static function to be a representation of the hydrostatic buoyancy force.

D. Kolmogorov-Gabor Polynomial Model (Nonlinear)

The final model considered in this paper utilises a polynomial nonlinearity, which results in a Kolmogorov-Gabor polynomial (KGP) model [17].

. In this case, Equation (1) becomes:

$$f_E(k) = \sum_{i=1}^{n_a} a_{i1} f_E(k-i) + \sum_{i=0}^{n_b} b_{i1}\eta(k-n_d-i)$$
$$+ \; \ldots$$
$$+ \sum_{i=1}^{n_a} a_{ip} f_E^p(k-i) + \sum_{i=0}^{n_b} b_{ip}\eta^p(k-n_d-i)$$
$$+ \sum_{i=1}^{n_a} \sum_{j=0}^{n_b} c_{ij} f_E(k-i)\eta(k-n_d-j)$$
$$+ \; \ldots \tag{4}$$

where p is the maximum polynomial order for the terms involving η and f_E alone, as well as the cross-product terms.

The KGP model is a black box model having a nonlinear input-output relationship, but is linear in the parameters a_{ij}, b_{ij} and c_{ij}.

During the preparation of the present work, the presence of the cross-product terms in the model typically resulted in an instability in the identified KGP model. For this reason, the cross-product terms in the model of Equation (4) have been removed, obtaining the simpler model:

$$f_E(k) = \sum_{j=1}^{p}\Big[\sum_{i=1}^{n_a} a_{ij} f_E^j(k-i) + \sum_{i=0}^{n_b} b_{ij}\eta^j(k-n_d-i)\Big] \tag{5}$$

The cancellation of the cross-product terms reduces the flexibility of the KGP model in describing the different nonlinear effects, nevertheless, the presence of the terms, involving η and f_E alone, guarantees the introduction of nonlinear effects and an improvement with respect to the linear ARX model.

III. NUMERICAL WAVE TANK

The NWT in this study is based on the open-source CFD software OpenFOAM. Details for the implementation of an OpenFOAM NWT for wave energy experiments can be found in [20].

A. NWT Experiments

Two different types of experiments are performed to provide the model identification data: the NWT Dynamic Experiments and the NWT Hydrostatic Force Experiments.

1) NWT Dynamic Experiment: This experiment involves holding the body fixed in the presence of input waves and measuring the resulting hydrodynamic force on the body. The excitation force is given by removing the hydrostatic force, experienced by the device at equilibrium, from the total measured hydrodynamic force. In a NWT, like in the open ocean or in a physical tank, measuring η at the WEC's centre of mass presents an issue, since the body occupies that position. A possible solution is the employment of techniques of spatial reconstruction of the wave field, using a group of sensors located in the proximity of the floating body, like LIDAR instruments or buoys [21]. In the NWT, the problem is overcome by performing the experiment in two stages. First, the input waves are generated and η at the desired position is measured without the body in the tank (see Fig. 6-a). Next, the
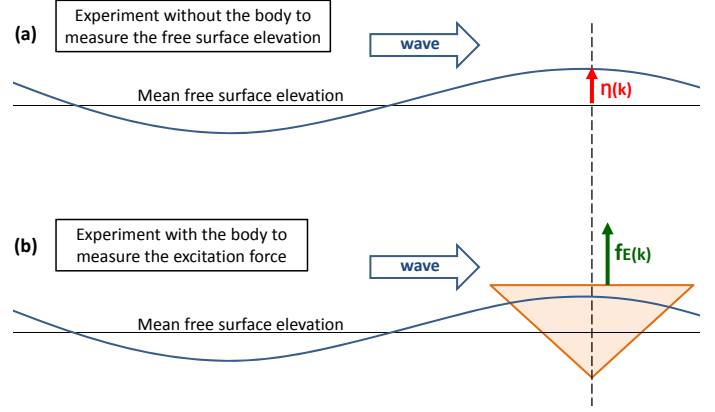

Fig. 6. NWT Hydrostatic Force Experiment: (a) the input waves are generated and the FSE at the desired position measured without the body. (b) the same input waves are generated but with the body geometry imported into the tank and held fixed while the resulting hydrodynamic force is measured.

same input waves are generated, but with the body geometry imported into the tank and held fixed, while the resulting hydrodynamic force on the body is measured, (see Fig. 6-b). Two vectors are produced by this experiment for model identification, one containing the FSE, $\{\eta_d(k)\}$, and the other the resulting excitation force, $\{f_{Ed}(k)\}$. Since this experiment is used to identify the dynamic of the system under study, it is important that the input signal $\{\eta_d(k)\}$ has a rich frequency content.

2) NWT Hydrostatic Force Experiment: This experiment is used to identify the static curve of the Hammerstein model. Two vectors are produced by this experiment for model identification, one containing the FSE, $\{\eta_s(k)\}$, and the other the resulting excitation force, $\{f_{Es}(k)\}$. Since in the previous NWT Dynamic Experiment the output signal $\{f_{Ed}(k)\}$ shows simultaneously the effects of the nonlinear static curve and of the system dynamics, it is difficult to separate one effect form the other one for the identification of the Hammerstein sub-blocks. As explained in Section II-C, the static curve of the Hammerstein model is related to the buoyancy force applied on the floating body, therefore, it is possible to design a specific experiment (the NWT Hydrostatic Force Experiment) to reveal only the buoyancy characteristics of the floating body and use them for the identification of the static curve. In this case, differently from the NWT Dynamic Experiment, the input signal $\{\eta_s(k)\}$ has to be slow so that dynamic effects are negligible and only the hydrostatic force is present in the excitation force measurement. Ideally, the body is held fixed and η is very slowly increased from the bottom to the top of the body and the resulting hydrostatic force is measured. However, in terms of implementing the experiment in the NWT, it is easier to keep the water level constant and slowly submerge the body, to obtain the same hydrostatic force measurements.
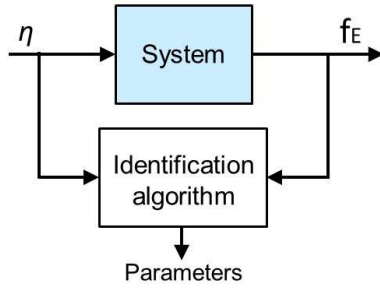
Fig. 7. System identification principle.

IV. MODEL IDENTIFICATION

A. System Identification

The fundamental idea of system identification is represented in Fig. 7. The identification procedure is based on a sequence of steps:

1) A parametric structure of the model is chosen (linear or nonlinear),

2) A suitable input signal is applied to excite the system, and

3) Using the recorded input and output signals, an identification algorithm is used to determine the optimal model parameters θ (the target is to minimize some error metric between the measured output y and the output $\hat{y}$ predicted by the identified parametric model).

B. Linear Regression and Least Squares

Consider a model with an output, $\hat{z}$, that is a linear combination of p independent variables, x_i:

$$\hat{z} = \theta_1 x_1 + \cdots + \theta_p x_p \tag{6}$$

where the coefficients, θ_i, are the unknown parameters [17].

It will be assumed that, $i = 1..N$ data samples, $\{z(i)\}$, have been measured. The error at each sample is $\varepsilon(i) = z(i) - \hat{z}(i)$. In matrix form:

$$\boldsymbol{\varepsilon} = \mathbf{z} - \hat{\mathbf{z}} = \mathbf{z} - \mathbf{X}\boldsymbol{\theta} \tag{7}$$

where:

$$\boldsymbol{\varepsilon} = \begin{bmatrix} \varepsilon(1) & \varepsilon(2) & ... & \varepsilon(N) \end{bmatrix}^T, \tag{8}$$

$$\mathbf{z} = \begin{bmatrix} z(1) & z(2) & ... & z(N) \end{bmatrix}^T, \tag{9}$$

$$\hat{\mathbf{z}} = \begin{bmatrix} \hat{z}(1) & \hat{z}(2) & ... & \hat{z}(N) \end{bmatrix}^T, \tag{10}$$

$$\mathbf{X} = \begin{bmatrix} x_1(1) & x_2(1) & ... & x_p(1) \\ x_1(2) & x_2(2) & ... & x_p(2) \\ \vdots & \vdots & \ddots & \vdots \\ x_1(N) & x_2(N) & ... & x_p(N) \end{bmatrix}, \tag{11}$$

$$\boldsymbol{\theta} = \begin{bmatrix} \theta_1 & \theta_2 & ... & \theta_p \end{bmatrix}^T. \tag{12}$$

$\mathbf{X}$ and $\mathbf{z}$, are called the data matrix and the observation vector respectively. In a full column rank context, the estimated parameters that minimize the least squares error are [17]:

$$\hat{\boldsymbol{\theta}} = \underset{\theta}{argmin}(\boldsymbol{\varepsilon}^T \boldsymbol{\varepsilon}) = (\mathbf{X}^T\mathbf{X})^{-1}\mathbf{X}^T\mathbf{z}. \tag{13}$$

The least squares problem is not usually resolved calculating the solution directly from Equation (13), because the use of $\mathbf{X}^T\mathbf{X}$ increases the possibility to obtain an ill-conditioned problem (the condition number of $\mathbf{X}^T\mathbf{X}$ is approximately the square of the condition number of the data matrix $\mathbf{X}$). Instead, a QR factorization method was implemented, which allows computing the least square solution directly from $\mathbf{X}$ without forming $\mathbf{X}^T\mathbf{X}$ [22] [23].

If the parameters have also to satisfy the linear equality constraints $\mathbf{A}\boldsymbol{\theta} = \mathbf{d}$, the estimated parameters are:

$$\hat{\boldsymbol{\theta}}_c = \hat{\boldsymbol{\theta}} - \mathbf{H}^{-1}\mathbf{A}^T(\mathbf{A}\mathbf{H}^{-1}\mathbf{A}^T)^{-1}(\mathbf{A}\hat{\boldsymbol{\theta}} - \mathbf{d}), \tag{14}$$

where $\mathbf{H} = \mathbf{X}^T\mathbf{X}$, and $\hat{\boldsymbol{\theta}}$ is calculated via Equation (13) [17].

C. Time Delay and Dynamical Order Estimation (n_d, n_a, n_b)

An important part of the model structure selection is the choice of the delay n_d and the dynamical orders n_a and n_b. As Equation (1) suggests, $y(k)$ is a function of n_a output and $n_b + 1$ input values, taken at different time instants. Once n_a, n_b and n_d are selected, it is possible to obtain the different model structures (for this paper ARX, Hammerstein and KGP) by changing the function $g()$. Since linear and nonlinear models share the same n_a, n_b and n_d, all these parameters are estimated implementing a trial and error process on several ARX models having different n_a, n_b and n_d and their performances measured with a loss function (a measure of the modelling error). For each ARX model estimation, independent training and validation data sets are utilised. At the end, the simplest ARX model able to repeat the validation data with a sufficient accuracy is selected (parsimonious model) [24].

D. ARX Model Identification

Performing the NWT Dynamic Experiment (see Section III-A), the signals $\{\eta_d(k)\}$ and $\{f_{Ed}(k)\}$ for $i = 1...N$, are generated, and they can be utilised as input and output for the identification of the ARX model. The first possible predicted model output is for $k = \tau + 1$ (the first τ values of the output data are utilised as initial conditions), where $\tau = max\{n_a, (n_b + n_d)\}$. The last possible predicted model output is for $k = \widetilde{N}$, where

$$\widetilde{N} = \begin{cases} N & \text{if } n_d \geq 0, \\ N + n_d & \text{if } n_d < 0. \end{cases}$$

In this case, Equations (9), (11) and (12) become:

$$\mathbf{z} = \begin{bmatrix} f_{Ed}(\tau + 1) & f_{Ed}(\tau + 2) & ... & f_{Ed}(\widetilde{N}) \end{bmatrix}^T, \tag{15}$$

$$\mathbf{X} = \begin{bmatrix} f_{Ed}(\tau) & ...f_{Ed}(\tau+1-n_a) & \eta_d(\tau+1-n_d)...\eta_d(\tau+1-n_d-n_b) \\ f_{Ed}(\tau+1) & ...f_{Ed}(\tau+2-n_a) & \eta_d(\tau+2-n_d)...\eta_d(\tau+2-n_d-n_b) \\ \vdots & \ddots \quad \vdots & \vdots \qquad \ddots \qquad \vdots \\ f_{Ed}(\widetilde{N}-1) & ... \quad f_{Ed}(\widetilde{N}-n_a) & \eta_d(N) \qquad ... \qquad \eta_d(N-n_b) \end{bmatrix}$$

$$\hat{\boldsymbol{\theta}}_{\mathbf{arx}} = \begin{bmatrix} a_1 & a_2 & ... & a_{n_a} & b_0 & b_1 & ... & b_{n_b} \end{bmatrix}^T. \tag{16}$$

respectively. The estimated parameters are determined from Equation (13).

E. Hammerstein Model Identification

The first step, in the identification of the Hammerstein model, is to identify the nonlinear static block. The nonlinear static function can be approximated with a linear combination of basis functions; in this way, it is possible to apply linear regression for the identification. For simplicity, the selected basis functions in this paper are polynomials $\{x^0, x^1, x^2, ..., x^{n_c}\}$. Therefore, the relationship between the input and the output of the nonlinear static block is:

$$\hat{s}(k) = c_1\eta(k) + c_2\eta^2(k) + ... + c_{n_c}\eta^{n_c}(k) \qquad (17)$$

where, $c_0 = 0$ is imposed (if the FSE is zero, the applied excitation force has to be zero). Under static conditions $s(k) = f_E(k)$ (a consequence of the DC_{gain} of the ARX equal to one). Therefore, Equation (17) becomes:

$$\hat{f}_E(k) = \sum_{i=1}^{n_c} c_i\eta^i(k) \qquad (18)$$

The NWT Hydrostatic Force Experiment (see Section III-A) generates the signals $\{\eta_s(k)\}$ and $\{f_{Es}(k)\}$, that can be utilised as input and output for the identification of the nonlinear static block. In this case, Equation (6) becomes Equation (18) and Equations (9), (11) and (12) become:

$$\mathbf{z} = \begin{bmatrix} f_{Es}(1) & f_{Es}(2) & ... & f_{Es}(N) \end{bmatrix}^T \qquad (19)$$

$$\mathbf{X} = \begin{bmatrix} \eta_s^1(1) & \eta_s^2(1) & ... & \eta_s^{n_c}(1) \\ \eta_s^1(2) & \eta_s^2(2) & ... & \eta_s^{n_c}(2) \\ \vdots & \vdots & \ddots & \vdots \\ \eta_s^1(N) & \eta_s^2(N) & ... & \eta_s^{n_c}(N) \end{bmatrix} \qquad (20)$$

$$\hat{\theta}_{\mathbf{Hc}} = \begin{bmatrix} c_1 & c_2 & ... & c_{n_c} \end{bmatrix}^T \qquad (21)$$

respectively. The estimated parameters are determined from Equation (13). The identification of $\hat{\theta}_{\mathbf{Hc}}$ is repeated for different values of n_c, evaluating the fitting error of the static function. Lastly, the smallest n_c that leads to a fitting error smaller than 3% is selected (as a good compromise between parsimony and accuracy), together with the associated $\hat{\theta}_{\mathbf{Hc}}$.

In the second step, the ARX block is identified utilising the signals $\{\eta_d(k)\}$ and $\{f_{Ed}(k)\}$, generated with the NWT Dynamic Experiment. Now that $\theta_{\mathbf{Hc}}$ is known, it is possible to calculate the output $\{s(k)\}$ of the nonlinear static block using Equation (17). In this way, both the input and the output of the ARX model is known, and it is therefore possible to identify the ARX parameters $\theta_{H_{ARX}}$, under the constraint that the DC gain of the ARX is equal to one: $DC_{gain} = (\sum_{i=1}^{n_b} b_i)/(1 + \sum_{i=1}^{n_a} a_i) = 1$, which corresponds to an equality constraint on the parameters $\mathbf{A} = [-1, -1, ..., -1, 1, 1, ...1]$ and $d = 1$. In this case Equations (9), (11) and (12) become:

$$\mathbf{z} = \begin{bmatrix} f_{Ed}(\tau+1) & f_{Ed}(\tau+2) & ... & f_{Ed}(\widetilde{N}) \end{bmatrix}^T, \qquad (22)$$

$$\mathbf{X} = \begin{bmatrix} f_{Ed}(\tau) & ...f_{Ed}(\tau+1-n_a) & s(\tau+1-n_d)...s(\tau+1-n_d-n_b) \\ f_{Ed}(\tau+1) & ...f_{Ed}(\tau+2-n_a) & s(\tau+2-n_d)...s(\tau+2-n_d-n_b) \\ \vdots & \ddots & \vdots & \vdots & \ddots & \vdots \\ f_{Ed}(\widetilde{N}-1) & ... & f_{Ed}(\widetilde{N}-n_a) & s(N) & ... & s(N-n_b) \end{bmatrix}$$
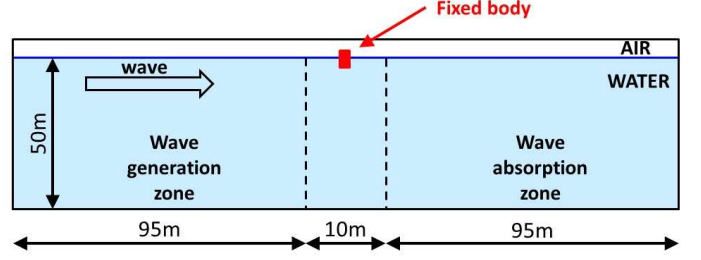

Fig. 8. Wave tank geometry.

$$\hat{\theta}_{\mathbf{Harx}} = \begin{bmatrix} a_1 & a_2 & ... & a_{n_a} & b_0 & b_1 & ... & b_{n_b} \end{bmatrix}^T \qquad (23)$$

respectively. The estimated parameters are given from Equation (14).

F. Kolmogorov-Gabor Polynomial Model Identification

For the KGP model, the NWT Dynamical Experiment signals are utilised, obtaining from Equations (9) and (12):

$$\mathbf{z} = \begin{bmatrix} f_{Ed}(\tau+1) & f_{Ed}(\tau+2) & ... & f_{Ed}(\widetilde{N}) \end{bmatrix}^T,$$

$$\hat{\theta}_{\mathbf{KGP}} = [a_{11},...,a_{n_a 1},b_{01},...,b_{n_b 1},...,a_{1p},...,a_{n_a p},b_{0p},...,b_{n_b p}]^T$$

Each of the $(\widetilde{N} - \tau)$ rows of the data matrix (11) has the form: $[f_{Ed}(k-1),...,f_{Ed}(k-n_a), \eta(k-n_d),...,\eta(k-n_d-n_b),...,f_{Ed}^p(k-1),...,f_{Ed}^p(k-n_a), \eta^p(k-n_d),...,\eta^p(k-n_d-n_b)]$, where $k = (\tau+1),...,N$.

V. ILLUSTRATIVE EXAMPLES

In this section, the methods described in Sections II- IV are implemented on different test devices. The present case study considers a two dimensional (2D) NWT, whereby the NWT is one cell thick and symmetry planes are imposed on the front and back faces of the domain. The 2D NWT is used to allow a timely investigation of the optimal experiment design, before moving to the much computationally slower 3D NWT for real WEC geometries. The NWT is a 50m deep tank with walls 100m from the device and with wave creation/absorption implemented via the waves2FOAM package [25] utilising two 95m long relaxation zones situated 5m either side of the device (see Fig. 8). Since two dimensional (2D) NWT simulations are utilised, the geometries of the test devices are infinitely long horizontal bars, having vertical cross-sections of a triangle, a circle and a box, with the dimensions shown in Fig. 9. For all the geometries, the draft is 50% of the device height. In the context of 2D NWT simulations, the waves move along a direction perpendicular to the infinitely long horizontal body axis, therefore, no wave directionality effects on the body are investigated.

A. Model Training and Identification

As illustrated in Section III-A, for the model identification, two kinds of NWT experiments are performed for each geometry, NWT Hydrostatic Force Experiment and NWT Dynamic Experiment, generating output data vectors sampled at $Ts = 0.1$s.
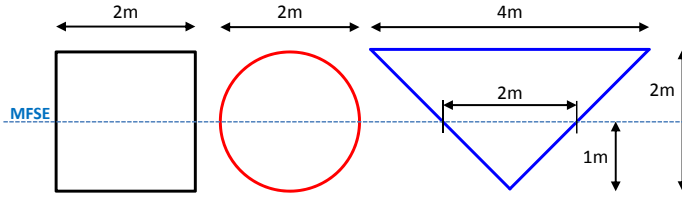
Fig. 9. Test device geometries: box, circle and triangle. The dotted line represents the mean free surface elevation (MFSE).
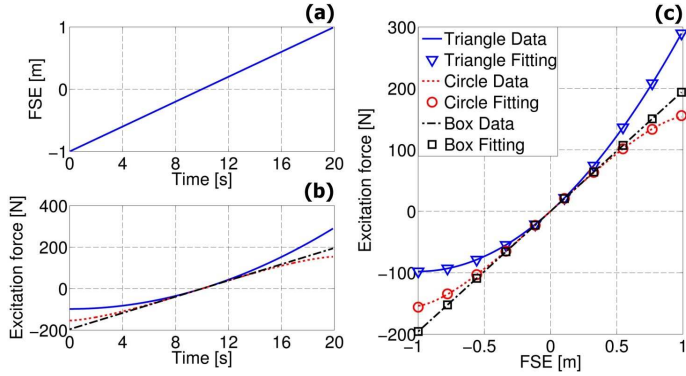

Fig. 10. Results from the NWT Static Force Experiment and fitting of the Hammerstein's static curves in case of triangle ($n_c = 2$), circle ($n_c = 3$) and box ($n_c = 1$).

The results from the NWT Static Force Experiments are shown in Figure 10. Figure 10-(a) shows the FSE, starting from the bottom of the device and slowly rising, until the device is completely submerged. Figure 10-(b) shows the excitation force on the body during this FSE change. Figure 10-(c) then plots the excitation force as a function of the FSE, showing the nonlinear nature of the relationship for the triangular and circular geometries.

Figure 11 shows the fitting error of the static curves of the Hammerstein models as a function of n_c, and the identified values of n_c for the different geometries (n_c equal to 1, 2 and 3 for box, triangle and circle respectively). Figure 10-(c) shows
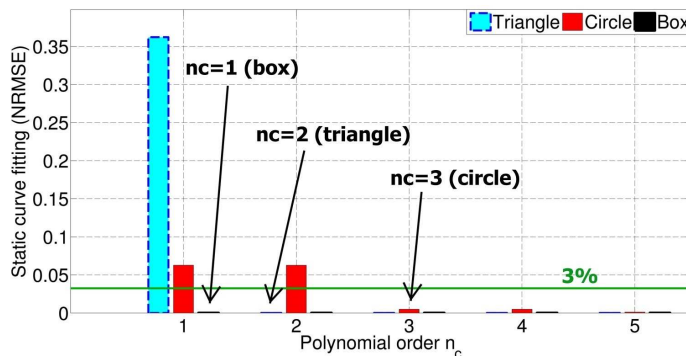

Fig. 11. The fitting error of the static curve of the Hammerstein model for different polynomial order n_c. The smallest n_c is chosen that guarantees fitting error smaller than 3%. In case of the box, the static curve is a straight line, therefore the fitting error is already zero for $n_c = 1$
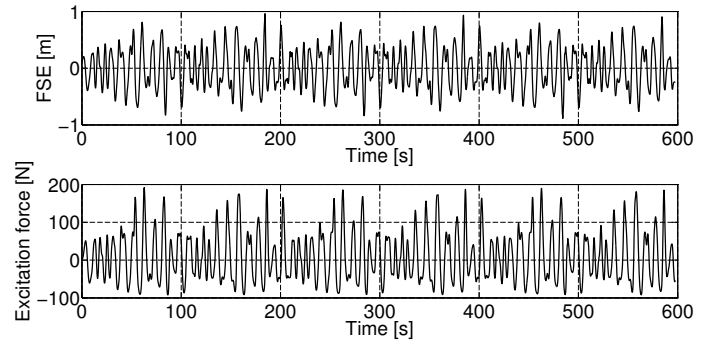

Fig. 12. Training experiment T1.

TABLE I
IDENTIFIED n_a, n_b, n_d, n_c AND p FOR THE TRIANGLE, CIRCLE AND BOX GEOMETRIES.

Geometry	n_a	n_b	n_d	n_c	p
Triangle	4	2	-8	2	2
Circle	3	2	-6	3	2
Box	3	2	-7	1	2

the fitting of the static curves of the Hammerstein models.

For the simulation of the NWT Dynamic Experiments, two different sea states have been utilised, having Jonswap spectra characterised by: ($H_s = 1.5$m, $T_p = 10$s) and ($H_s = 0.5$m, $T_p = 10$s). Each sea state realization has been obtained as multisine signal, consisting of 100 harmonics with a fundamental frequecncy of 0.01Hz and selecting a random phase for each harmonic.

For each sea state, four different realizations have been generated (in total 8 realizations), and utilised with each geometry (in total 24 experiments). The experiments involving the triangle have been called Ti with $i = 1, ...8$, and similarly, the symbols Ci and Bi have been utilised for the experiments involving circle and box geometry respectively (see Tables II, III and IV). Fig. 12 shows the experiment T1 utilised to train the models for the triangular geometry, where it is possible to see that, the FSE has been intentionally constructed in a way so, that the device is never overtopped or dried out.

Utilising the strategy illustrated in Section IV-C, the input delay time n_d, and the dynamical orders n_a and n_b have been identified for the three geometries; the results are summarized in Table I. In the case of the circular geometry, Fig. 13 shows the loss function calculated for the different ARX models, obtained by changing n_d. It is possible to see that the minimum value occurs for $n_d = -6$ (noncausal ARX model). In Fig. 14 the loss function is plotted for different values of n_a, for the case of circular geometry. It is possible to see that, for n_a bigger than 3, the loss function has no significant reduction, indicating that $n_a = 3$ is appropriate for the identification of a parsimonious model.

The polynomial order of the KGP model $p = 2$ has been identified, observing that bigger values of p improve the training fitting but degrade the quality of the validation fitting (overfitting).
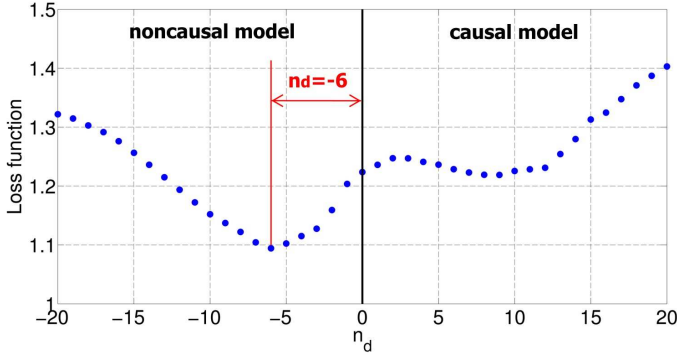
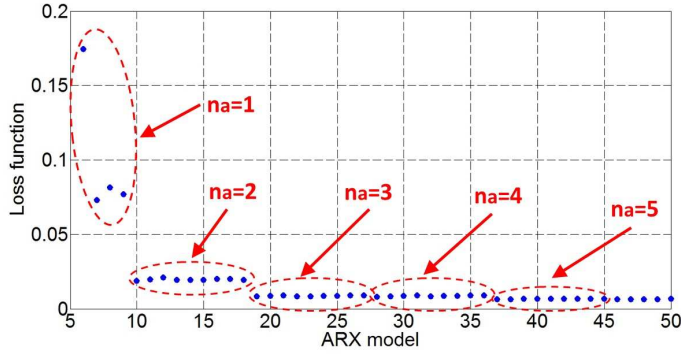Fig. 13. Determination of $n_d = -6$, for the circle geometry.

Fig. 14. Determination of the dynamical order $n_a = 3$, for the circle geometry.
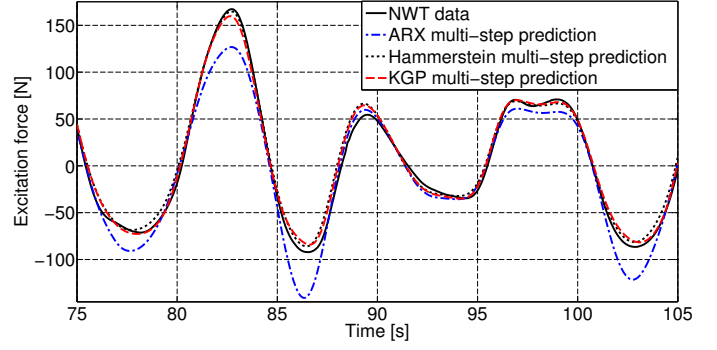

Fig. 15. Identified model performances on the training experiment T1. The multi-step model predictions are compared with the training data.

TABLE II
NRMSE MODELS MULTI-STEP PERFORMANCES FOR TRAINING (TRIANGLE).

Training Experiment	ARX	Hammerstein	KGP
H_s=1.5m ; T_p=10s ; ($T1$)	0.2336	0.1011	0.0891
H_s=1.5m ; T_p=10s ; ($T2$)	0.2388	0.1028	0.0972
H_s=1.5m ; T_p=10s ; ($T3$)	0.2705	0.1078	0.1060
H_s=1.5m ; T_p=10s ; ($T4$)	0.2488	0.1099	0.0960
H_s=0.5m ; T_p=10s ; ($T5$)	0.0915	0.0681	0.0450
H_s=0.5m ; T_p=10s ; ($T6$)	0.0819	0.0697	0.0483
H_s=0.5m ; T_p=10s ; ($T7$)	0.1017	0.0697	0.0506
H_s=0.5m ; T_p=10s ; ($T8$)	0.0803	0.0676	0.0421

presence of nonlinear effects in the data.

B. Model Validation

The simplest way to evaluate the accuracy of a model is to identify it on training data, and then, evaluate its performance on test data from a different experiment. A model, which fits

Different error metrics can be utilised to compare the model prediction $\hat{f}_E(k)$ with the measured signal $f_E(k)$. A possible choice could be the mean square error (MSE), but it is not normalised with respect to the magnitude of $f_E(k)$. To overcome this inconvenience, the mean absolute percentage error (MAPE) could be chosen. However, drawback of this error metric is that it can give a distorted picture of the error, if there are zero or nearly-zero values in the measured signal. Since $f_E(k)$ oscillates around zero, there is a good possibility that it could happen. This leads to the definition of a new metric, which we term normalised root mean-squared error (NRMSE):

$$NRMSE = \frac{\sqrt{\sum_k [f_E(k) - \hat{f}_E(k)]^2}}{\sqrt{\sum_k f_E^2(k)}} \qquad (24)$$

Fig. 15 shows, for experiment T1, the multi-step predictions of the identified ARX, Hammerstein and KGP models. It is possible to see that none of the modelling approaches is perfect, but the linear model has particular difficulty in following peaks in the excitation force. All the fitting results on the training experiments are summarised in Table II, III and IV for the triangle, circle and box, respectively. It is possible to observe that, for all 24 experiments, in the case of training fitting, the KGP model shown to be the best, followed by the Hammerstein and finally the ARX model, confirming the

TABLE III
NRMSE MODELS MULTI-STEP PERFORMANCES FOR TRAINING (CIRCLE).

Training Experiment	ARX	Hammerstein	KGP
H_s=1.5m ; T_p=10s ; ($C1$)	0.1233	0.1135	0.0922
H_s=1.5m ; T_p=10s ; ($C2$)	0.1324	0.1151	0.0967
H_s=1.5m ; T_p=10s ; ($C3$)	0.1495	0.1228	0.1117
H_s=1.5m ; T_p=10s ; ($C4$)	0.1430	0.1222	0.1072
H_s=0.5m ; T_p=10s ; ($C5$)	0.0371	0.0351	0.0306
H_s=0.5m ; T_p=10s ; ($C6$)	0.0366	0.0366	0.0261
H_s=0.5m ; T_p=10s ; ($C7$)	0.0372	0.0359	0.0304
H_s=0.5m ; T_p=10s ; ($C8$)	0.0351	0.0340	0.0273

TABLE IV
NRMSE MODELS MULTI-STEP PERFORMANCES FOR TRAINING (BOX).

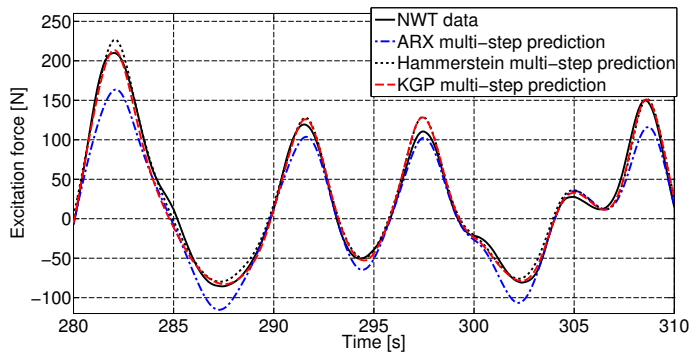| Training Experiment	ARX	Hammerstein	KGP
H_s=1.5m ; T_p=10s ; ($B1$)	0.1311	0.1270	0.0961
H_s=1.5m ; T_p=10s ; ($B2$)	0.1294	0.1251	0.0914
H_s=1.5m ; T_p=10s ; ($B3$)	0.1368	0.1308	0.0952
H_s=1.5m ; T_p=10s ; ($B4$)	0.1259	0.1243	0.0917
H_s=0.5m ; T_p=10s ; ($B5$)	0.0531	0.0481	0.0463
H_s=0.5m ; T_p=10s ; ($B6$)	0.0591	0.0561	0.0477
H_s=0.5m ; T_p=10s ; ($B7$)	0.0547	0.0511	0.0493
H_s=0.5m ; T_p=10s ; ($B8$)	0.0537	0.0494	0.0448

Fig. 16. Identified model performances on the validation experiment $T2$. The multi-step model predictions are compared with the training data. The models have been trained on the experiment $T1$.

Validation Experiment	ARX	Hammerstein	KGP
H_s=1.5m; T_p=10s; ($T2$)	0.2394	0.1017	0.0894
H_s=1.5m; T_p=10s; ($T3$)	0.2697	0.1071	0.1042
H_s=1.5m; T_p=10s; ($T4$)	0.2514	0.1084	0.0999
H_s=0.5m; T_p=10s; ($T5$)	0.1050	0.0643	0.0718
H_s=0.5m; T_p=10s; ($T6$)	0.0960	0.0649	0.0775
H_s=0.5m; T_p=10s; ($T7$)	0.1123	0.0657	0.0713
H_s=0.5m; T_p=10s; ($T8$)	0.0954	0.0638	0.0759

well the training data, is not necessary a good model on a different experiment (overfitting problem). In this paper, instead of validating the identified model on a singular experiment, it has been decided to stress the model with an intense group of 7 validation tests. In this way, it is possible to obtain a more complete overview regarding the ability of the model in predicting the excitation force in different wave conditions. Considering the triangular geometry, the models trained on T1 are validated on all the other experiments T2...T8, with the fitting results summarised in Table V. Fig. 16 shows the performance of the models trained with experiment T1 and validated with experiment T2. Analogous procedures have been done for the circle and box, with the results shown in Table VI and VII. In general, the models show the ability to predict a different realization belonging to the same sea state or to another sea state (the model trained with $H_s = 1.5$m behaves well also for $H_s = 0.5$m). This indicates a parsimonious structure for the models and a good estimate for the parameters. Furthermore, it is possible to see that, in most cases, the nonlinear models (and particularly the KGP model) are able to predict the excitation force with more accuracy. Therefore, it is possible to conclude that the problem under investigation includes nonlinearities, and that the nonlinear identified models are able to describe them.

In Fig. 17, the identified models from experiment T1 (triangular geometry) have been also validated on an experiment with a monochromatic wave of 0.1Hz. It can be seen that the fully nonlinear NWT simulation exhibits an asymmetric output, with respect to the MFSE, in response to the symmetrical

Validation Experiment	ARX	Hammerstein	KGP
H_s=1.5m; T_p=10s; ($C2$)	0.1216	0.1114	0.0887
H_s=1.5m; T_p=10s; ($C3$)	0.1374	0.1194	0.1224
H_s=1.5m; T_p=10s; ($C4$)	0.1311	0.1174	0.1115
H_s=0.5m; T_p=10s; ($C5$)	0.0722	0.0556	0.0545
H_s=0.5m; T_p=10s; ($C6$)	0.0730	0.0561	0.0533
H_s=0.5m; T_p=10s; ($C7$)	0.0718	0.0553	0.0547
H_s=0.5m; T_p=10s; ($C8$)	0.0726	0.0558	0.0534

Validation Experiment	ARX	Hammerstein	KGP
H_s=1.5m; T_p=10s; ($B2$)	0.1278	0.1243	0.0934
H_s=1.5m; T_p=10s; ($B3$)	0.1317	0.1277	0.0984
H_s=1.5m; T_p=10s; ($B4$)	0.1383	0.1332	0.0992
H_s=0.5m; T_p=10s; ($B5$)	0.0747	0.0761	0.0662
H_s=0.5m; T_p=10s; ($B6$)	0.0805	0.0826	0.0692
H_s=0.5m; T_p=10s; ($B7$)	0.0771	0.0777	0.0691
H_s=0.5m; T_p=10s; ($B8$)	0.0769	0.0786	0.0665

sinusoidal η, owing to the fact that the triangle's geometry is asymmetric to respect to the MFSE. It is not possible for the linear ARX model to replicate this nonlinear behaviour and it is outperformed by the nonlinear models that are able to replicate the asymmetric output. This is confirmed also in the results in Table II and V, where the fitting of the ARX model is poor, in particular for the sea state with $H_s = 1.5$m. This is because the nonlinear effects, arising from the geometric asymmetries, become more relevant with larger waves.

VI. Conclusion

Three different discrete time model structures have been introduced to model the relationship between FSE and excitation force, all linear with respect to the parameters, offering the advantage of a convex optimisation for parameters that can be easily solved.

The models were tested on three different geometries, and the superiority of the nonlinear models (Hammerstein and
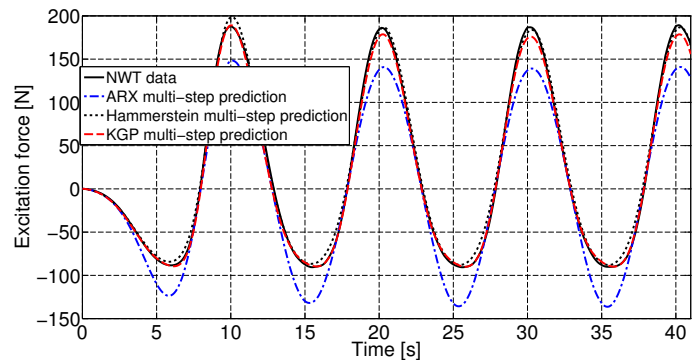

Fig. 17. Model trained with experiment T1, and validated on monochromatic experiment with f=0.1Hz.

KGP models) showed the nonlinear nature of the investigated problem.

The linear ARX model exhibited strong limitations due to its inability to generate asymmetry at its output, for a stimulation with a symmetric input. The nonlinear models, on the other hand, shown a very good ability in asymmetry generation.

The identified nonlinear models display good performance both in training and validation, indicating that the selected model structures, the estimated parameters and the identification procedures are appropriate. Overall, the KGP model behaves as the most accurate model, both in training and validation.

REFERENCES

[1] W. Cummins, "The impulse response function and ship motions," DTIC Document, Tech. Rep., 1962.

[2] J. Davidson, S. Giorgi, and J. V. Ringwood, "Numerical wave tank identification of nonlinear discrete time hydrodynamic models," *RENEW2014*, 2014.

[3] J. Ringwood, G. Bacelli, and F. Fusco, "Energy-maximizing control of wave-energy converters: The development of control system technology to optimize their operation," *Control Systems, IEEE*, vol. 34, no. 5, pp. 30–55, Oct 2014.

[4] P. Kracht, S. Perez-Becker, J.-B. Richard, and B. Fischer, "Performance improvement of a point absorber wave energy converter by application of an observer-based control: Results from wave tank testing."

[5] P. Moraal and J. Grizzle, "Observer design for nonlinear systems with discrete-time measurements," *Automatic Control, IEEE Transactions on*, vol. 40, no. 3, pp. 395–404, 1995.

[6] J. Ringwood, J. Davidson, and S. Giorgi, "Optimising numerical wave tank tests for the parametric identification of wave energy device models," in *Prof. 34th Int. Conf. on Ocean, Offshore and Arctic Engineering (OMAE)*. ASME, 2015.

[7] A. S. Zurkinden, F. Ferri, S. Beatty, J. P. Kofoed, and M. Kramer, "Nonlinear numerical modeling and experimental testing of a point absorber wave energy converter," *Ocean Engineering*, vol. 78, pp. 11–21, 2014.

[8] J. Falnes, "On non-causal impulse response functions related to propagating water waves," *Applied Ocean Research*, vol. 17, no. 6, pp. 379–389, 1995.

[9] A. Babarit and P. Laporte-Weywada, "On the numerical modelling of the nonlinear behaviour of a wave energy converter," *Proceedings of OMAE2009*, 2009.

[10] M. Guérinel, M. Alves, and A. Sarmento, "Nonlinear modelling of the dynamics of a free floating body," *EWTEC, Southampton*, 2011.

[11] M. Lawson, Y.-H. Yu, A. Nelessen, K. Ruehl, and C. Michelen, "Implementing nonlinear buoyancy and excitation forces in the wec-sim wave energy converter modeling tool," in *ASME 2014 33rd International Conference on Ocean, Offshore and Arctic Engineering*. American Society of Mechanical Engineers, 2014, pp. V09BT09A043–V09BT09A043.

[12] J.-C. Gilloteaux, G. Bacelli, and J. Ringwood, "A non-linear potential model to predict large-amplitudes-motions: application to a multi-body wave energy converter," 2008.

[13] L. Ljung, *System Identification: Theory for the User*, 2nd ed. Prentice Hall PTR, Upper Saddle River, NJ, USA, 1999.

[14] Ljung, "Perspectives on system identification," *Annual Reviews in Control*, vol. 34, no. 1, pp. 1–12, 2010.

[15] G. Rao and H. Unbehauen, "Identification of continuous-time systems," *IEE Proceedings-Control Theory and Applications*, vol. 153, no. 2, pp. 185–220, 2006.

[16] J. Davidson, S. Giorgi, and J. V. Ringwood, "Linear parametric hydrodynamic models for ocean wave energy converters identified from numerical wave tank experiments," *Ocean Engineering*, vol. 103, pp. 31–39, 2015.

[17] O. Nelles, *Nonlinear System Identification: From Classical Approaches to Neural Networks and Fuzzy Models*. Springer, Berlin Heidelberg, Germany, 2001.

[18] R. K. Pearson and M. Pottmann, "Gray-box identification of block-oriented nonlinear models," *Journal of Process Control*, vol. 10, p. 301315, 2000.

[19] E.-W. Bai, "Decoupling the linear and nonlinear parts in Hammerstein model identification," *Automatica*, vol. 40, pp. 671–676, 2003.

[20] J. Davidson, M. Cathelian, L. Guillemet, T. l. Huec, and J. V. Ringwood, "Implementation of an openfoam numerical wave tank for wave energy experiments," *EWTEC2015*, 2015.

[21] F. Paparella, K. Monk, V. Winands, M. Lopes, D. Conley, and J. V. Ringwood, "Benefits of up-wave measurements in linear short-term wave forecasting for wave energy applications," in *Control Applications (CCA), 2014 IEEE Conference on*. IEEE, 2014, pp. 2048–2053.

[22] G. Golub and C. Van Loan, *Matrix Computations*, 4th ed., ser. Matrix Computations. Johns Hopkins University Press, Baltimore, Maryland, USA, 2012.

[23] T. Sauer, *Numerical Analysis*. Pearson Education, NY, USA, 2012.

[24] L. Ljung, *MATLAB System Identification Toolbox*. MathWorks, Natick, Massachusetts, USA, 2013.

[25] N. G. Jacobsen, D. R. Fuhrman, and J. Fredsøe, "A wave generation toolbox for the open-source cfd library: Openfoam®," *International Journal for Numerical Methods in Fluids*, vol. 70, no. 9, pp. 1073–1088, 2012.